The Proceedings of the International Conference on Creationism

Volume 4
Print Reference: Pages 303-314

Article 23

1998

Use of History Dependent Material Models for Simulating Geophysical Events Related to the Bible

Mark F. Horstemeyer

USE OF HISTORY DEPENDENT MATERIAL MODELS FOR SIMULATING GEOPHYSICAL EVENTS RELATED TO THE BIBLE

MARK F. HORSTEMEYER, PHD
5333 Lenore Ave, Livermore, CA 94550

KEYWORDS: anisotropy, olivine, glacial ice, internal state variable, constitutive equation

ABSTRACT

Computational models have played a key role for estimating ages related to large scale geologic events such as the Ice Age and Genesis flood. Embedded within the computational model is a critical component called the material model, which in many cases can be the most important feature of the calculation. Simple material models have been applied to assess the timing of the Ice Age and Genesis flood. To achieve higher accuracy for time predictions, more physically-based material models are necessary to simulate the complex rheological behavior. In this paper, an internal state variable (ISV) unified-creep-plasticity model that captures history effects of microstructural features within a material is presented to describe high confining pressure, deviatoric behavior of mantle rheology. Stress is not just a function of strain, strain rate, and temperature but is a function of the history of the microstructure as well. The thermodynamics and internal state variable hardening rate equations are presented. The ISV model is compared to power law creep for polycrystalline ice and polycrystalline olivine to illustrate that simple material models cannot predict behavior that is often experienced in complex boundary value problems, such as, trying to simulate creeping/surging Glacial ice or thermal runaway of the subducting lithosphere that may have occurred in the Genesis flood.

INTRODUCTION

Numerical modeling of subduction kinematics, plate tectonics, and glacial motion has been a tool of geophysical researchers to understand the geological past. Both evolutionists and creationists have approached these arenas with computational modeling, but neither camp has attempted to employ internal state variable (ISV) constitutive models to determine the timing of these geological events. A critical issue in determining the current state of a material is the varying history of temperature, pressure, and loading conditions applied to the material. Hence, the constitutive model, or rheological model, should be able to capture history effects if one were to assess the current state of the material. One such constitutive modeling framework that can capture the changing temperature, pressure, and deformation histories is the ISV modeling framework. The internal state of a material is represented by rate equations that reflect underlying microstructural rearrangements that change with temperature, pressure, and deformation and in-turn influence macroscale mechanical properties. Internal state variable models have successfully been used to reflect histories of brittle and ductile engineering materials as well as monophase and multiphase materials.

ISV theory has been seldom used for modeling geomaterials, yet finite deformation analysis of the upper mantle of the earth and glacial ice requires that a model be able to capture deviatoric deformation effects from temperature, pressure, strain rate, and deformation histories. The most commonly used material model to simulate the inelastic deviatoric response of the mantle has been that of power law creep (which is not an ISV theory) with an emphasis on different values of the hardening exponent, coefficient, and activation energy [cf. Kirby, 1973, 1983; Goetze, 1978; Karato and Toriumi, 1989; Chopra and Paterson, 1981, 1984]. More recently, Covey-Crump [1994] has employed the use of the Hart internal state variable model [1970, 1976] to study the mechanical properties of Carrara Marble. Auburtin et al. [1992] have used an ISV model to model creep of ice. In this writing, the Bammann [1985, 1988, 1990] ISV model is applied to model the deviatoric response of olivine (which comprises a majority of the upper mantle), Lherzolite (which is 60-70% olivine), and glacial ice. In the first section, the constitutive equations for the Bammann ISV model are discussed. A non-unique set of

material constants for olivine experiments and glacial ice are then determined and presented.

Tensor notation is used extensively in this writing so definitions are warranted. An underscore indicates a first rank tensor (a vector) with a small letter and a second rank tensor with a capital letter, i.e. $\underline{v}$ and $\underline{F}$, respectively. A double underscore on a capital letter indicates a fourth rank tensor, $\underline{\underline{C}}$. A global Cartesian coordinate system is assumed so no distinction is made between the contravariant and covariant components. A first, second, and fourth rank tensor in the Einsteinian indicial notation are given by v_i, F_{ij}, and C_{ijkl}, respectively. The summation convention over repeated indices is implied, for example, $\sigma_{ii} = \sigma_{11} + \sigma_{22} + \sigma_{33}$. In general, for any tensor variable x, $\overset{\circ}{x}$ represents the corotational derivative. The tensorial dyadic product is denoted by $\otimes$, for example, $\underline{v} \otimes \underline{v}$ is a second rank tensor. The second and third invariants of deviatoric stress are denoted by J_2 and J_3 and the deviatoric overstresses by J_2^* and J_3^*, respectively.

CONSTITUTIVE EQUATIONS

Because the most used constitutive equation for mantle materials has been the power law form with temperature dependence, it is worthwhile discussing the differences between the power law equation and the ISV equations. The power law material constants are generally determined by creep tests and describe microstructural behavior in a somewhat heuristic manner. Although not usually shown in tensorial form, equation (1) shows the power law creep formula as a second rank tensor,

$$\underline{D}^{in} = A\frac{3}{2}\exp\left(\frac{-Q}{RT}\right)\sigma^n \underline{e}, \tag{1}$$

where A is the power law coefficient, n is the power law exponent, σ is the stress, $\underline{e}$ is the unit direction tensor, Q is the activation energy, R is the universal gas constant, T is absolute temperature, and $\underline{D}^{in}$ is the inelastic rate of deformation (creep rate). Though not used much in the geophysics community, a form of the inelastic rate of deformation was developed by Garofalo (1963) to capture a broader range of inelastic behavior (the power law regime and power law breakdown regime) by using a hyperbolic sine for the stress dependence,

$$\underline{D}^{in} = A\frac{3}{2}\exp\left(\frac{-Q}{RT}\right)\sinh\left(\frac{\sigma}{B}\right)\underline{e}, \tag{2}$$

where B is considered a drag stress parameter.

The power law and Garofalo models inherently assume isotropic material behavior. Therefore no texture or kinematic (anisotropic) hardening arising from directional dislocation substructures is considered, although anisotropy clearly arises in geomaterials under finite deformations. Another shortcoming of these models is that they include no elasticity. Fundamentally, elastic-plastic couplings cause the mechanical stress state and are important especially when nonmonotonic loading sequences arise. Covey-Crump (1994) insightfully argued that the physical meaning of the material constants for the power law and Garofalo equations is lacking and therefore can lead to unreliable extrapolations outside of those cases tested. As such, they cannot be used in a general sense to solve boundary value problems. However, ISV formulations will have less of a problem with extrapolation, because they are more closely tied to microstructural behavior. Finally and most importantly, equations (1)-(2) do not include history effects from temperature, pressure, or deformation, even though all real materials are functions of their history.

Internal State Variable Formulation

Thermodynamically-based internal state variable constitutive equations that are used to capture history effects are cast in two classes. The first class uses hereditary integrals: that the present state of the material depends on the present values and past history of observable variables. The second class is based on the

concept that the present state of the material depends only on the present values of observable variables and a set of internal state variables (ISVs). The second approach is maintained by the author to be more appropriate to solve a wide range of boundary value problems, and it is this form that is discussed in this writing.

The notion of internal state was introduced into thermodynamics by Onsager [1931] and was applied to continuum mechanics by Eckart [1940, 1948]. The ISV formulation is a means to capture a representative volume element response instead of the complex details of the local microstructural response; hence, the ISV averages over lower spatial length scales without describing all the details of the microscopic arrangement. The notion is that the complete microstructure arrangement is unnecessary as long as the macroscale ISV representation is complete. As a result, the ISV must be based on first principles and physically observed behavior, and the laws of thermodynamics must be considered in developing the ISV approach [Coleman and Gurtin, 1967; Kestin and Rice, 1970]. From the viewpoint of rational thermodynamics, the ISVs provide the additional information necessary for a rational description of the thermodynamic state of the material. From the viewpoint of thermodynamics of irreversible processes, the ISVs provide the information required to describe neighboring constrained equilibrium states.

The Helmholtz free energy is decomposed into the free energy associated with thermoelastic strain, ψ^{e}, and temperature as influenced by the ISVs and the free energy associated with inelasticity, ψ^{in}, according to

$$\psi = \psi^{e}\left(\underline{E}^{e}, T, \nabla_i T, \underline{V}_i\right) + \psi^{in}\left(\underline{V}_i, T, \nabla_i T\right), \tag{3}$$

where $\underline{E}$ is the thermoelastic Green strain and T is the absolute temperature. These two variables are termed **observable state variables**. The $\underline{V}_i$ are the **internal state variables** associated with **effects** of microstructural rearrangement and not with the actual geometrical rearrangement of microstructure. The index i is a counter for each of the number of ISVs represented. Effectively, the ISV is a lower order reflection of higher order microstructural phenomena occurring at lower spatial length scales. The ISVs are sometimes referred to as generalized displacements. Each of the ISVs can be represented by any order of tensor rank, but its thermodynamic conjugate must be the identical order. By defining the Helmholtz free energy in this manner, thermodynamic conjugate forces arise [Chaboche, 1972; Germain et al., 1983; and Krajcinovic, 1983] with respect to their generalized displacements in the Bammann ISV model as

$$\hat{\underline{\sigma}} = \rho\frac{\partial \psi}{\partial \underline{E}},\ \Lambda = -\rho\frac{\partial \psi}{\partial T},\ \underline{b} = -\rho\frac{\partial \psi}{\partial \underline{\alpha}},\ \kappa = -\rho\frac{\partial \psi}{\partial R},\ \varphi = -\rho\frac{\partial \psi}{\partial D},\ \frac{\partial \psi}{\partial \nabla_i T} = 0 \tag{4}$$

where $\hat{\underline{\sigma}}$ is the second Piola-Kirchhoff stress defined with respect to the stress-free configuration, Λ is the specific entropy, $\underline{b}$ is the backstress tensor corresponding to kinematic hardening, κ is the scalar isotropic stress corresponding to isotropic hardening, and ϕ is the energy release rate corresponding to the damage variable. The density, ρ, corresponds to the stress-free configuration in which these relations are written.

The equations used within the context of the finite element method are the rate of change of the observable and internal state variables given by,

$$\overset{\circ}{\underline{\sigma}} = \dot{\underline{\sigma}} - \underline{W}^{e}\underline{\sigma} - \underline{\sigma}\underline{W}^{e} = \lambda(1-D)tr\left(\underline{D}^{e}\right)\underline{I} + 2\mu(1-D)\underline{D}^{e} - \frac{\dot{D}}{1-D}\underline{\sigma} \tag{5}$$

$$\underline{D}^{e} = \underline{D} - \underline{D}^{in}. \tag{6}$$

$$\underline{D}^{in} = f(T)\sinh\left[\frac{\|\underline{\sigma}' - \underline{\alpha}\| - \{R + Y(T)\}\{1-D\}}{V(T)\{1-D\}}\right]\frac{\underline{\sigma}' - \underline{\alpha}}{\|\underline{\sigma}' - \underline{\alpha}\|}, \tag{7}$$

$$\overset{\circ}{\underline{\alpha}} = \dot{\underline{\alpha}} - \underline{W}^{e}\underline{\alpha} + \underline{\alpha}\underline{W}^{e} = h(T)\underline{D}^{in} - \left[\sqrt{\frac{2}{3}}r_d(T)\|\underline{D}^{in}\| + r_s(T)\right]\|\underline{\alpha}\|\underline{\alpha}, \tag{8}$$

$$\dot{R} = H(T)\underline{D}^{in} - \left[\sqrt{\frac{2}{3}}R_d(T)\|\underline{D}^{in}\| + R_s(T)\right]R^2, \tag{9}$$

$$\dot{D} = \sqrt{\frac{2}{3}} \sinh\left[\frac{2(2n-1)I_1}{3(2n+1)\sqrt{3J_2}}\right]\left[\frac{1}{(1-D)^n} - (1-D)\right]\left\|\underline{D}^{in}\right\|, \tag{10}$$

and are generally written as objective rates ($\overset{o}{\underline{\sigma}}, \overset{o}{\underline{\alpha}}$) with indifference to the continuum frame of reference assuming a Jaumann rate in which the continuum spin equals the elastic spin ($\underline{W} = \underline{W}^e$). The ISV rate equations (8)-(10) are functions of the observable variables (temperature, stress state, and rate of deformation). In general, the rate equations of generalized displacements, or thermodynamics fluxes, describing the rate of change may be written as independent equations for each ISV or as derivatives of a suitably chosen potential function arising from the hypothesis of generalized normality [Rice, 1971]. An advantage of assuming generalized normality, although somewhat restrictive, is unconditional satisfaction of the Kelvin inequality of the second law of thermodynamics (nonnegative intrinsic dissipation), i.e.

$$\underline{\sigma}:\underline{D}^{in} - \underline{b}:\overset{0}{\underline{\alpha}} - \kappa \bullet \dot{R} - \phi \bullet \dot{D} \geq 0. \tag{11}$$

Although generalized normality is not an appropriate assumption for surface rocks, it is appropriate for examining mantle rocks since dilational effects that affect nonnormality are negated by high confining pressures. In the experiments examined and in materials within the mantle, deviatoric responses dominate.

The selection of the ISVs may, in principle, be somewhat arbitrary, but the kinematic hardening, isotropic hardening, and damage rate equations are physically motivated and strongly influence the history of the material. The Bammann ISV model accounts for deviatoric inelastic deformation resulting from the presence of dislocations in crystallographic material, dilatational deformation, and ensuing failure from growth of microdamage. Microdamage can be represented by porosity or microcracking and will reduce the material strength, enhance the inelastic flow, and soften the elastic moduli.

In equation (6), the elastic Lame constants are denoted by λ and μ. The elastic rate of deformation ($\underline{D}^e$) results when the total deformation ($\underline{D}$), which is defined by the boundary conditions, is subtracted from the flow rule as shown in equation (6).

The independent variables for the inelastic rate of deformation are given in equation (7) as the stress, temperature, and internal state variables. This is similar to power law and Garofalo equations for creep except that the ISVs are now included. The deviatoric inelastic flow rule, $\underline{D}^{in}$, encompasses the regimes of creep and plasticity. It is a function of the temperature, the kinematic hardening internal state variable ($\underline{\alpha}$), the isotropic hardening internal state variable (R), the volume fraction of damaged material (D), and the functions $f(T)$, $V(T)$, and $Y(T)$, which are related to yielding with Arrhenius-type temperature dependence. The function $Y(T)$ is the rate-independent yield stress. The function $f(T)$ determines when the rate-dependence affects initial yielding. The function $V(T)$ determines the magnitude of rate-dependence on yielding. These functions are determined from simple isothermal compression tests with different strain rates and temperatures,

$$V(T) = C_1 \exp\left(-C_2/T\right),\ Y(T) = C_3 \exp\left(C_4/T\right),\ f(T) = C_5 \exp\left(-C_6/T\right). \tag{12}$$

The kinematic hardening internal state variable, $\underline{\alpha}$, reflects the effect of anisotropic dislocation density, and the isotropic hardening internal state variable R, reflects the effect of the global dislocation density. As such, the hardening equations (8)-(9) are cast in a hardening-recovery format that includes dynamic and static recovery. The functions $r_s(T)$ and $R_s(T)$ are scalar in nature and describe the diffusion-controlled static or thermal recovery, while $r_d(T)$ and $R_d(T)$ are scalar functions describing dynamic recovery. Hence, the two main types of recovery that are exhibited by populations of dislocations within olivine or ice are captured in the ISVs. The anisotropic hardening modulus is $h(T)$, and the isotropic hardening modulus is $H(T)$.

The hardening moduli and dynamic recovery functions account for deformation-induced anisotropy arising from texture and dislocation substructures by means of stress-dependent variables. Texture is prolific in mantle materials [Kirby and Konenberg, 1987]. Miller and McDowell [1992] showed that by using J_3^* in the hardening equations the different hardening rates between axisymmetric compression and torsion (torsional softening) were accurately captured. Miller et al. [1995] and Horstemeyer [1995, 1996] included this feature in the Bammann ISV model as

$$r_d(T) = C_7\left(1+C_{19}\left[\frac{4}{27}-\frac{J_3^{*2}}{J_2^{*3}}\right]\right)\exp\left(-C_8/T\right), \tag{13}$$

$$h(T)=\left\{C_9\left(1+C_{20}\left[\frac{4}{27}-\frac{J_3'^{2}}{J_2'^{3}}\right]\right)\right\}-C_{10}T, \tag{14}$$

$$r_s(T)=C_{11}\exp\left(-C_{12}/T\right), \tag{15}$$

$$R_d(T) = C_{13}\left(1+C_{21}\left[\frac{4}{27}-\frac{J_3^{*2}}{J_2^{*3}}\right]\right)\exp\left(-C_{14}/T\right), \tag{16}$$

$$H=\left\{C_{15}\left(1+C_{22}\left[\frac{4}{27}-\frac{J_3'^{2}}{J_2'^{3}}\right]\right)\right\}-C_{16}T, \tag{17}$$

$$R_s(T)=C_{17}\exp\left(-C_{18}/T\right), \tag{18}$$

where $J_2' = \frac{1}{2}(\underline{\sigma}'-\underline{\alpha})^2$ and $J_3' = \frac{1}{3}(\underline{\sigma}'-\underline{\alpha})^3$. The deviatoric stress $\underline{\sigma}'$ is expressed in indicial notation as

$$\sigma_{ij}' = \sigma_{ij} - \frac{1}{3}\sigma_{ii}. \tag{19}$$

Two illustrations of history effects using the Bammann ISV model are shown in Figures 1 and 2. Figure 1 [Bammann, 1985] shows jump rate tests performed on 304L stainless steel. Two tests were performed at constant, isothermal strain rates ($5e10^{-5}$/sec and $5e10^{-2}$/sec). The third test was performed at a strain rate of $5e10^{-5}$/sec first up to 5% strain and then to a strain rate of $5e10^{-2}$/sec after 5% strain. As Figure 1 illustrates for the jump test, the stress-strain curve rises above the constant 10^{-3}/sec strain rate curve. Hence, the strain rate history changes the current stress state of the material. The Bammann ISV model captures this response, but a power law creep model or equation of state model would jump to the previous curve with a strain rate of $5e10^{-2}$/sec. Figure 2 [Bammann et al., 1996] demonstrates a temperature jump test from 800C to 20C for 304L stainless steel. Again, the Bammann ISV model captured the temperature history effect, but a power law or equation of state model would jump from the 800C curve to the 20C curve.

The damage variable D represents the damage fraction of material within a continuum element. The mechanical properties of a material depend upon the amount and type of microdefects within its structure. Deformation changes these microdefects, and when the number of microdefects accumulates, damage is said to have grown. The notion of a damaged state in continuum field theory emerged when Kachanov [1958] introduced a damage variable to describe the microdefect density locally in a creeping material. The idea was that damage could be measured by the volume fraction of voids under creep conditions. Rabotnov [1963] furthered this notion with an rate equation of void density.

By including damage, D, as an ISV, different forms of damage can be represented. Equation (10) introduces the void volume fraction (porosity) as damage. The upper mantle experiences very large confining pressures, where deviatoric deformation dominates and dilatational deformation is typically not present (dilatational effects relate to porosity level). However, Bercovici [1996] has recently included porosity in upper mantle analysis of plate subduction related to water effects and lubrication. It may be conceivable that microdefects such as cracking and porosity are present in the presence of high rate plate subduction in

which water plays an important role. More experimental work needs to be performed to evaluate these speculations.

The generalized thermodynamic force conjugate, ϕ, is often referred to as the energy release rate for elastic brittle materials and the J-integral for inelasticity. In essence, an increment of damage will have associated energy released per unit damage extension as new damaged area (or volume) is developed. A representative volume element of solid material with pores/cracks, or damage, will experience a reduction in the material strength, an enhanced inelastic flow, and decreased elastic moduli as damage grows. When the damage reaches a critical value, failure occurs. Different damage rules can easily be incorporated into the constitutive framework. Bammann et al. [1990; 1993] and Horstemeyer [1992, 1993] have demonstrated the applicability of the Cocks and Ashby [1980] void growth rule used as the damage rate equation in the Bammann model.

The Cocks and Ashby [1980] spherical void growth rule was derived based on power law and diffusion controlled creep. The porosity scalar evolution is shown in equation (10). The parameter n is described in the Cocks-Ashby framework as the inverse of the strain rate sensitivity. The parameter n is used as a phenomenological damage parameter determined empirically from notched tensile tests or notched creep tests. The first invariant in equation (10) is defined by

$$I_1 = tr\left(\tilde{\sigma}' - \frac{2}{3}\tilde{\alpha}'\right). \tag{20}$$

DETERMINATION OF BAMMANN MODEL CONSTANTS FOR OLIVINE

Experimental data for high confining pressure tests for initially isotropic wet and dry polycrystalline olivine are used to determine the Bammann ISV model constants. The temperature dependent elastic moduli from the Preliminary Reference Earth Model (Dzeiwonski and Anderson, 1981) can be used for olivine throughout the mantle. Stress-strain data for a range of temperatures from 1273K<T<1573K were analyzed to determine the yield functions, hardening moduli, and dynamic recovery functions for wet and dry Anita Bay dunite (Chopra and Paterson, 1981, 1984) as shown in Figures 3 and 4. Creep data from Chopra and Paterson (1981, 1984) up to 1573K was used to determine the static recovery constants. Nonmonotonic data from Chopra and Paterson (1984) for dry olivine was used to illustrate the changing strain rate history and ability of the ISV model to capture the effect as illustrated in Figure 5. Lherzolite data (Carter and Ave'Lallemant, 1970) were also examined for nonmonotonic strain rate sequences. Lherzolite is a fine-grained nearly equiaxed granular rock comprising 60%-70% olivine, 20%-30% enstatite, 5%-10% diopside, and less than 1% spinel.

The differences between wet and dry olivine are not just based upon the wet olivine comprising another material phase. Complex chemical and mechanical responses arise when olivine contains water. For example, Karato et al. (1986) observed that wet olivine experiences much more grain growth than the dry olivine. Grain growth will affect the hardening/softening rate of the material. A tie also exists between the porosity level and grain growth mechanisms. Furthermore, recrystallization plays a role on deformation for wet olivine, but dry olivine experiences neither grain growth nor recrystallization.

Figure 3 shows the correlation of the model to the wet monolithic polycrystalline olivine experimental data. Some kinematic hardening and static recovery was assumed. The grain size was approximately 100mm, and no molten material was present. The volume fraction of water was 10%. The data reveals a strong temperature dependence. A nonlinear regression correlating the model with test data revealed that the mean error was 2% and the peak error 8%. Table 1 shows the proposed material constants for wet and dry olivine. Constants C2, C6, C12, C18, C20-C25 are assumed to be zero for this parameter determination.

Figure 4 shows the correlation of the model to the dry monolithic polycrystalline olivine experiments. Some kinematic hardening and static recovery was assumed as well. We also assumed the same amount of strain rate sensitivity on the yield function as in the wet olivine case. The grain size was approximately 100mm, no molten material was present, and no water was present. A nonlinear regression revealed that the mean error was 3% and the peak error 6%. No determination of the damage parameter was performed for wet or dry olivine due to the lack of experimental data.

Figure 5 shows a good correlation with changing strain rates from at 1300C. More experiments with changing temperatures and a broader range of strain rates would be beneficial.

Figure 6 shows a comparison of the ISV model to eight different temperatures and three different strain rates for Lherzolite. Figure 7 illustrates the usefulness of the model by capturing the nonmonotonic strain rate history effect on the stress-strain response.

Table 1. Bammann material constants for wet and dry polycrystalline olivine.

Material constants	wet olivine	dry olivine
C_1 (MPa)	2.2e1	2.2e1
C_3 (MPa)	2.0e1	2.0e1
C_4 (K)	1.398e3	1.398e3
C_5 (1/sec)	2.e-5	2e-5
C_7 (1/MPa)	1.329e4	2.744e-2
C_8 (K)	1.995e5	0
C_9 (MPa)	2.935e4	4.512e4
C_{10} (K)	2.08e1	0
C_{11} (sec/MPa)	5e-7	4.521e-5
C_{13} (1/MPa)	1.52e6	1.55e10
C_{14} (K)	1.982e4	3.8e4
C_{15} (MPa)	7.039e4	1.72e5
C_{16} (K)	4.047e1	1.08e2
C_{17} (sec/MPa)	0	4.984e-6
C_{19}	2.597e-2	2.597e-2
C_{20}	1.398e3	1.398e3

DETERMINATION OF BAMMANN MODEL CONSTANTS FOR GLACIAL ICE

Glacial ice and sea ice are examined in the context of the Bammann ISV model. A complete set of experimental data for glacial ice is not currently available to uniquely determine the Bammann ISV model constants, but strain rate and temperature experimental data of Hawkes and Mellor (1972), Haynes (1978), and Cox et al. (1984) were used to account for the temperature and rate-dependent parameters. These experiments were performed under high confining pressures such that only the deviatoric response was analyzed. It is to be noted that Aubertin (1992) has used a simpler form of an internal state variable model for polycrystalline ice and has suggested that the Bammann model be evaluated. Table 2 summarizes the glacial ice model constants. Figure 5 shows that the strain rates ranged from 10^{-3}/sec to 10^{-7}/sec, and the temperature ranged from 223K to 268K. Data were not available to accurately determine the hardening behavior, hence, a linear plastic modulus was assumed. As such, many of the constants are assumed to be zero correlating to perfect plasticity or power law creep. For the sea ice, properties determined by Yang (1983) were used to determine model constants for yield and hardening behavior. Table 3 summarizes the model constants for sea ice. As for glacial ice, many constants are assumed to be zero. Softening experienced by sea ice arises from microcracking operating on the stress state. Damage, as stated earlier, is included in the modeling framework, but not in the form of microcracking so no model comparison to experimental data is shown. This is an area of future research.

Table 2. Bammann material constants for polycrystalline glacial ice in compression.

Material constants	ice
C_1 (MPa)	3.02e-5
C_2 (K)	-2744
C_3 (MPa)	9.56
C_4 (K)	-478.9
C_5 (1/sec)	1e-5
C_{15} (MPa)	1.0

Table 3. Bammann material constants for polycrystalline columnar sea ice in tension.

Material constants	ice
C_1 (MPa)	0.02911
C_3 (MPa)	0.2
C_5 (1/sec)	2.097e-4
C_7 (1/MPa)	700
C_9 (MPa)	2581
C_{11} (sec/MPa)	0.006685
C_{13} (1/MPa)	722
C_{15} (MPa)	9723.1
C_{17} (sec/MPa)	1.8616

SUMMARY

A constitutive model is introduced that has the ability to accurately track history effects of complex nonlinear geomaterials, such as mantle olivine and glacial ice, and hence could give more accurate simulations of Biblical geophysical events. Material constants were determined for wet and dry olivine, glacial ice, and sea ice which were tested under different strain rates and temperatures, but more exhaustive experiments are needed to examine the pressure, time, strain rate, and deformation histories of mantle materials. These material constant sets can be used to solve numerical boundary value problems related to the flood.

Acknowledgment The author is grateful for the encouragement and review of this document from John Baumgardner, David McDowell, and Bruce Kistler.

REFERENCES

[1] Auburtin, M., *Cold Regions Science and Technology*, V20, N2:225-227, 1992.
[2] Bammann, D. J., The Mechanics of Dislocations, ASM, p. 203, 1985.
[3] Bammann, D. J., *Modelling and Control of Casting and Welding Processes IV*, eds. Giamei, A. F. and Abbaschian, G. J. TMS Pub., Warrendale, PA, 1988.
[4] Bammann, D.J., *Appl. Mech. Rev.*, Vol. 1, pp. 312-318, 1990.
[5] Bammann, D.J., Chiesa, M.L., McDonald, A., Kawahara, W.A., Dike, J.J., Revelli, V.D., *Failure Criteria and Analysis in Dynamic Response*, ed. H.E. Lindberg, ASME AMD, Vol. 107, pp. 7-12, Nov. 1990.
[6] Bammann, D. J., Chiesa, M. L., Horstemeyer, M. F., and Weingarten, L. I., *Structural Crashworthiness and Failure*, ., eds. N. Jones and T. Weirzbicki, Elsevier Applied Science, 1993.
[7] Bammann, D.J. et al., 2nd Int. Conf. on Quenching and the Control of Distortion, Cleveland, OH, 1996.
[8] Bercovici, D., *Earth and Planetary Science Letters*, V.14, N1-2:41, 1996.

[9] Carter, N.L. and Ave'Lallemant, H.G, *Geological Society of America Bulletin*, v.81, p. 2181, 1970.
[10] Chaboche, J.L., *These Univ. Paris VI*, publication ONERA, N 1978-3, 1972.
[11] Chopra, P.N. and Paterson, M.S., *Tectonophysics*, Vol. 78, pp. 453-473, 1981.
[12] Chopra, P.N. and Paterson, M.S., *J. Geophysical Research*, Vol. 89, No. B9, pp. 7861-7876, 1984.
[13] Cocks, A. C. F., Ashby, M. G., *Metal Science*, Aug-Sept, pp. 395-402, 1980.
[14] Coleman, B. D., Gurtin, M. E. , *J. Chem.Phys.,* Vol. 47, pp. 597, 1967.
[15] Covey-Crump, S.J., *J. Geophys. Res.*, Vol. 99, No. B10, pp. 19793-19808, 1994.
[16] Cox, G. F. N., Richter-Menge, J. A., Weeks, W. F., Mellor, M., and Bosworth, H., CRREL Report, *Mechanical Properties of Multi-year Ice, Phase 1: Test Results*, 1984.
[17] Dziewonski, A.M. and Anderson, D.L., *Physics of Earth and Planetary Interiors*, Vol. 25, pp. 297-356, 1981.
[18] Eckart, C., *Phys. Rev.,* Vol. 58, pp. 267, 1940.
[19] Eckart, C., *Phys. Rev.*, Vol. 73, pp. 373, 1948.
[20] Garofalo, F., *Trans. Metall. Soc. AIME*, Vol. 227, pp. 351-356, 1963.
[21] Germain, P., Nguyen, Q.S., and Suquet, P., *J. Appl. Mech.,* vol. 50, pp. 1010-1020, 1983.
[22] Goetze, C., *Phil. Trans. R. Soc. Lond.,* Vol. 288 A, pp. 99-119, 1978.
[23] Hart, E.W., *Acta Metall.*, Vol. 18, pp. 599-610, 1970.
[24] Hart, E.W., *J. Enger. Mater. Tech.,* pp. 193-202, 1976.
[25] Hawkes, I. and Mellor, M., *J. Glaciology*, Vol. 11, No. 61, pp. 103-131, 1972.
[26] Haynes, F. D., *Effect of Temperature on the Strength of Snow Ice*, CRREL Report, 1978.
[27] Horstemeyer, M. F., *ASME AMD-Vol. 137, Advances in Local Fracture/Damage Models for the Analysis of Engineering Problems*, eds. J. H. Giovanola and A. J. Rosakis, 1992.
[28] Horstemeyer, M. F., *ASME-AMD-Vol. 171, Advances in Numerical Simulation Techniques for Penetration and Perforation of Solids*, eds. E. P. Chen and V. K. Luk, pp. 189-200, 1993.
[29] Horstemeyer, M. F., *Physically Motivated Modeling of Deformation-Induced Anisotropy,* PhD thesis, Georgia Institute of Technology, 1995.
[30] Horstemeyer, M. F., McDowell, D. L., Bammann, D. J., SAE Tech. Ser. 960599, ed. K. Chen, *Analysis of Autobody Stamping Technology*, 1996.
[31] Kachanov, L. M., *IVZ Akad. Nauk. S.S.R.,* Odt Tech Nauk No. 8, pp.26-31, 1958.
[32] Karato, S.I., Paterson, M.S., Fitzgerald, J.D., *J. Geophysical Research*, Vol. 91, No. B8, pp. 8151-8176, 1986.
[33] Karato, S.I. and Toriumi, M., *Rheology of Solids and of the Earth*, Oxford Science Publications, Oxford, 1989.
[34] Kestin, J. and Rice, J.R., *A Critical Review of Thermodynamics*, Mono Book Corp., Baltimore, MD, p. 275, 1970.
[35] Kirby, S.H., and Raleigh, *Tectonophysics*, Vol. 19, pp. 165-194, 1973.
[36] Kirby, S.H., *Reviews Geophys. Space Phys.*, Vol. 21, pp. 1458-1487, 1983.
[37] Kirby, S.H. and Kronenberg, A.K., *Reviews of Geophysics*, Vol. 25, No. 6, pp. 1219-1244, 1987.
[38] Krajcinovic, D., *J. Appl. Mech.,* vol. 50, pp. 355-360, 1983.
[39] Miller, M.P., McDowell, D.L., ASME Summer Applied Mechanics Meeting, Tucson, AZ, ASME AMD-Vol. 32, Microstructural Characterization in Constitutive Modeling of Metals and Granular Media, pp. 27-44, 1992.
[40] Miller, M. P, Bammann, D. J., Dawson, P., Simulation of Materials Processing: Theory, Methods and Applications, eds. Shen and Dawson, pp. 219-224, Balkema, Rotterdam, ISBN 90 5410 5534, 1995.
[41] Onsager, L., *Phys. Rev.,*Vol. 37, pp. 405; Vol. 38, pp. 2265, 1931.
[42] Rabotnov, I.N., *Progress in Applied Mechanics-The Prager Anniversary Volume*, pp. 307-315, 1963.
[43] Rice, J. R., *J. Mech. Phys. Solids*, Vol. 9, pp.433-455, 1971.
[44] Yang, W. S., *Trans. ASME J. Energy Res. Tech.*, V105, p. 2, 1983.

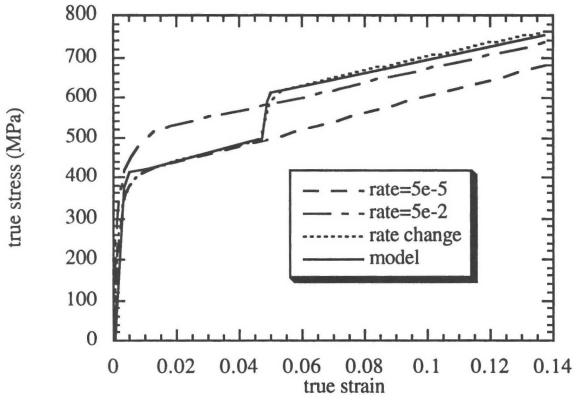

Figure 1. Comparison of model to jump rate tests for 304L stainless steel. Experimental data occurs at a strain rate of 0.00005 (s-1) where the temperature is nearly constant and at a strain rate of 0.05 (s-1) where the temperature increase is nearly adiabatic. The jump test changes rate at 0.05 strain. (D.J. Bammann, "An Internal State Variable Model of Elasto-Viscoplasticity," The Mechanics of Dislocations, eds. E.C. Aifantis and J.P. Hirth, American Society of Metals, PP. 203-212, 1985.)

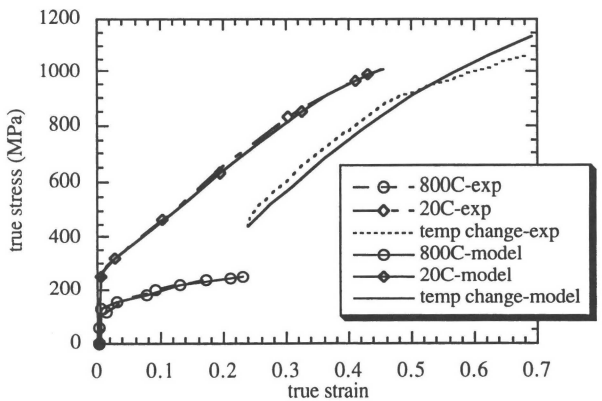

Figure 2. Comparison of model to jump temperature tests for 304L stainless steel. The jump in temperature occurs at 0.25 strain. (D.J. Bammann et al., "Development of a Carburizing and Quenching Simulation Tool: A Material Model for Carburizing Steels Undergoing Phase Transformations, 2nd Int. Conf. on Quenching and the Control of Distortion, Cleveland, OH, 1996.)

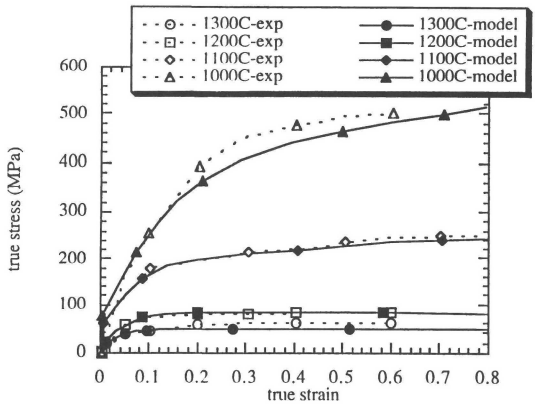

Figure 3. Comparison of model to wet polycrystalline olivine.

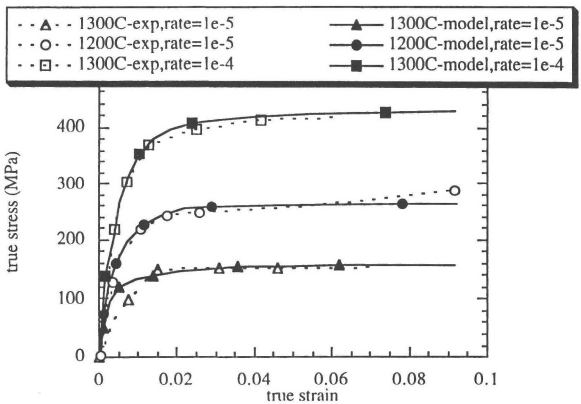

Figure 4. Comparison of model to dry polycrystalline olivine.

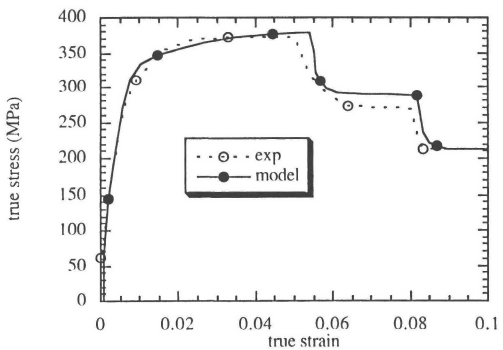

Figure 5. Comparison of model to dry polycrystalline olivine for varying strain rate history at 1300C.

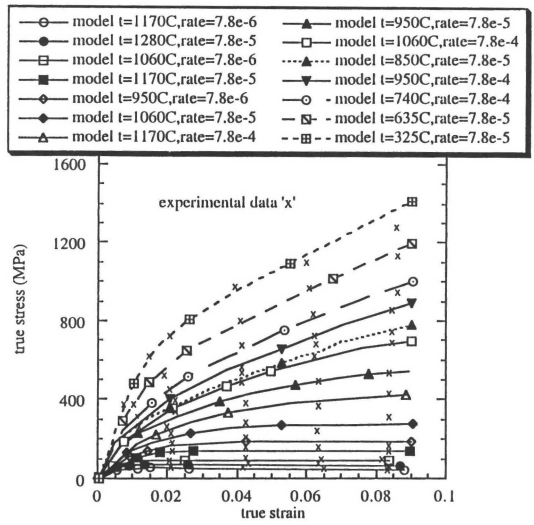

Figure 6. Comparison of model to Lherzolite.

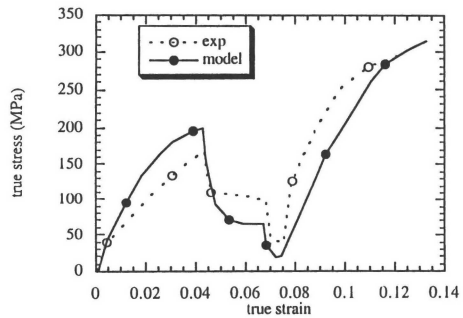

Figure 7. Comparison of model to Lherzolite for varying strain rate history at 1060C.

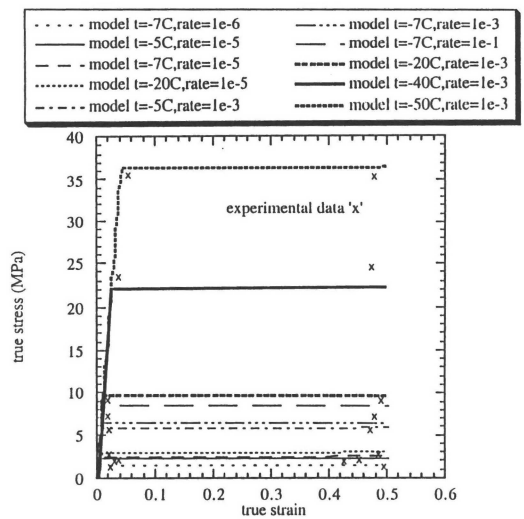

Figure 8. Comparison of model to glacial ice.